Targeting cancer addiction for SALL4 by shifting its transcriptome with a pharmacologic peptide

Article (Published Version)

Targeting cancer addiction for SALL4 by shifting its transcriptome with a pharmacologic peptide

Bee Hui Liu[a,1], Chacko Jobichen[a,b,1], C. S. Brian Chia[c], Tim Hon Man Chan[a], Jing Ping Tang[a], Theodora X. Y. Chung[a], Jia Li[a], Anders Poulsen[c,d], Alvin W. Hung[c], Xiaoying Koh-Stenta[c], Yaw Sing Tan[e], Chandra S. Verma[b,e,f], Hong Kee Tan[a,g], Chan-Shuo Wu[a], Feng Li[a], Jeffrey Hill[c], Joma Joy[c], Henry Yang[a], Li Chai[h,2], J. Sivaraman[b,2], and Daniel G. Tenen[a,i,2]

[a]Cancer Science Institute of Singapore, National University of Singapore, 117599 Singapore; [b]Department of Biological Sciences, National University of Singapore, 117543 Singapore; [c]Experimental Therapeutics Centre, Agency for Science, Technology and Research, 138669 Singapore; [d]Department of Chemistry, National University of Singapore, 117543 Singapore; [e]Bioinformatics Institute, Agency for Science, Technology and Research, 138671 Singapore; [f]School of Biological Sciences, Nanyang Technological University, 637551 Singapore; [g]National University of Singapore, Graduate School for Integrative Sciences and Engineering, 117456 Singapore; [h]Brigham and Women's Hospital, Harvard Medical School, Boston, MA 02115; and [i]Havard Stem Cell Institute, Harvard Medical School, Boston, MA 02115

Edited by Riccardo Dalla-Favera, Columbia University Medical Center, New York, NY, and approved June 4, 2018 (received for review January 22, 2018)

Sal-like 4 (SALL4) is a nuclear factor central to the maintenance of stem cell pluripotency and is a key component in hepatocellular carcinoma, a malignancy with no effective treatment. In cancer cells, SALL4 associates with nucleosome remodeling deacetylase (NuRD) to silence tumor-suppressor genes, such as PTEN. Here, we determined the crystal structure of an amino-terminal peptide of SALL4 (1–12) complexed to RBBp4, the chaperone subunit of NuRD, at 2.7 Å, and subsequent design of a potent therapeutic SALL4 peptide (FFW) capable of antagonizing the SALL4–NURD interaction using systematic truncation and amino acid substitution studies. FFW peptide disruption of the SALL4–NuRD complex resulted in unidirectional up-regulation of transcripts, turning SALL4 from a dual transcription repressor-activator mode to singular transcription activator mode. We demonstrate that FFW has a target affinity of 23 nM, and displays significant antitumor effects, inhibiting tumor growth by 85% in xenograft mouse models. Using transcriptome and survival analysis, we discovered that the peptide inhibits the transcription-repressor function of SALL4 and causes massive up-regulation of transcripts that are beneficial to patient survival. This study supports the SALL4–NuRD complex as a drug target and FFW as a viable drug candidate, showcasing an effective strategy to accurately target oncogenes previously considered undruggable.

SALL4 | RBBp4/NuRD | peptidomimetic | HCC | structural guided design

Sal-like 4 (SALL4) is a nuclear factor central to the maintenance of stem cell pluripotency (1–3), specifically expressed in fetal cells. SALL4 is down-regulated or absent in most adult tissues but is reactivated in solid (4–7) and hematological malignancies (8–11), often associated with poor prognosis (12–14). In embryonic stem cells, SALL4 forms a core transcriptional network with Oct4, Nanog, and Sox2 to drive embryonic stem cell (ESC) self-renewal (1–3). It was also observed that SALL4 plays a dual role in transcription activity in ESCs, activating self-renewal and repressing differentiation related transcripts at the same time (2, 15). Recently, we and others found that activation of SALL4 is a key driver in up to 55% of hepatocellular carcinoma (HCC) patients (14, 16, 17). It also serves as a biomarker for progenitor-like HCC (14, 16), an aggressive subset of HCC characterized by stem cell features, invasive potential, and poor patient prognosis (17). In HCC, we reported that the phosphatase and tensin homolog deleted on chromosome 10 (PTEN)–AKT-PI3K pathway is altered by the reexpression of SALL4 (16). Furthermore, we have also reported that SALL4 acts as a repressor of PTEN by recruiting the nucleosome remodeling deacetylase (NuRD) complex (18). NuRD is a chromatin remodeling complex that silences key regulators in ESCs and adult cells (19, 20); it has two independent enzymatic activities whereby nucleosomes are repositioned by the CDH3/4 ATPase subunits in order for the histone deacetylase (HDAC1/2) subunits to access their targets and repress target genes. The retinoblastoma binding protein 4 (RBBp4) is a subunit of NuRD. It is a WD40 repeat-containing protein, which consists of a seven-bladed β-propeller domain. In NuRD, RBBp4 acts as a chaperone in nucleosome assembly by bringing together histones H3 and H4 onto newly replicated DNA (21).

HCC is a fast-growing malignancy with a median survival of 11 mo. With less than 30% of patients able to receive potentially curative treatments like surgery and liver transplant, it is now the second leading cause of death worldwide (globocan.iarc.fr/) due to the lack of effective treatment options for the majority of HCC patients. The multikinase inhibitor Sorafenib is currently the first-line treatment available for patients with advanced HCC. However, this drug shows frequent adverse effects and only prolongs survival for an average of 3 mo (22). Promising new drugs that have reached clinical trials so far have met with failure. Therefore, there is an urgent need to explore alternative approaches for the treatment of this deadly disease. SALL4,

Significance

Hepatocellular carcinoma (HCC) is leading cause of death due to late discovery and lack of effective treatment. The finding of the Sal-like 4 (SALL4)–NuRD interaction in HCC opens a new therapeutic direction targeting an epigenetic regulator. Here, we identified the SALL4–NuRD binding site through structural resolution of the crystal complex, providing valuable insight for the development of antagonists against this interaction. Our subsequent design of a therapeutic peptide has demonstrated the possibility to develop a first-in-class drug targeting the SALL4–NuRD interaction in HCC. Furthermore, we discovered that the therapeutic peptide exhibits robust antitumor properties and works by inhibiting the repressive function of SALL4. Our work could also be beneficial to a broad range of solid cancers and leukemic malignancies with elevated SALL4.

Author contributions: B.H.L., C.J., C.S.B.C., C.S.V., J.H., J.J., H.Y., L.C., J.S., and D.G.T. designed research; B.H.L., T.H.M.C., J.P.T., T.X.Y.C., A.W.H., X.K.-S., Y.S.T., H.K.T., and F.L. performed research; B.H.L., C.J., C.S.B.C., and T.X.Y.C. contributed new reagents/analytic tools; B.H.L., C.J., J.L., A.P., and C.-S.W. analyzed data; and B.H.L., C.J., C.S.B.C., A.P., L.C., J.S., and D.G.T. wrote the paper.

The authors declare no conflict of interest.

This article is a PNAS Direct Submission.

Data deposition: The coordinates and structure factors of the RBBp4–SALL4 crystal complex have been deposited in the RCSB database, https://www.wwpdb.org/ (PBD ID code 5XWR). The RNA-seq and ChIP-seq data have been deposited in the Gene Expression Omnibus (GEO) database, https://www.ncbi.nlm.nih.gov/geo (accession no. GSE112729).

[1]B.H.L. and C.J. contributed equally to this work.

[2]To whom correspondence may be addressed. Email: lchai@bwh.harvard.edu, dbsjayar@nus.edu.sg, or csidgt@nus.edu.sg.

This article contains supporting information online at www.pnas.org/lookup/suppl/doi:10.1073/pnas.1801253115/-/DCSupplemental.

Published online July 5, 2018.

however, falls into the class of what is termed as "undruggable" targets, as a nuclear factor lacking a typical, druggable pocket for inhibitor binding. In this report, we discovered that the SALL4–NuRD interaction offers an intriguing potential therapeutic target, as SALL4 is expressed uniquely in a selected population of cancer cells with poor prognosis, and not in normal adult cells. Furthermore, we demonstrated that by targeting SALL4–NuRD, we are able to reverse the repression function of SALL4 in tumor-suppressor transcripts, switching SALL4 from a dual-mode transcription factor to single mode lacking transcriptional repression function. To that end, we resolved the RBBp4–SALL4(1–12) complex, determined key residues involved in the SALL4–RBBp4 binding, and designed a pharmacologic peptide (RRKFAKFQWI, named FFW hereafter) that blocked the interaction with high affinity, and reversed the repression function of SALL4 on target genes. The massive up-regulation of treatment-specific transcripts resulted in apoptosis, activation of tumor suppressors, and cell adhesion molecules, and subsequently showed a significant effect on inhibiting xenograft formation in mice. In addition, this report also highlights a viable and effective strategy incorporating structural analyses to accurately design a therapeutic approach against candidate genes that are otherwise considered undruggable.

Results

Structure of the SALL4–RBBp4 Complex. To target SALL4–NuRD interaction, we first determined the direct binding of SALL4(1–12) to RBBp4. We utilized the first 12 aa of SALL4 in isothermal titration calorimetry (ITC) assays to access the binding affinity of SALL4 to RBBp4, and found that the complex formed with a K_D of 1.04 ± 0.06 μM (Fig. 1*A*). These binding kinetics were further confirmed using surface plasmon resonance (SPR), with a calculated K_D for binding between the SALL4 peptide and RBBp4 of 1.5 μM (k_{on} = 16,830 ± 460 $M^{-1}s^{-1}$; k_{off} = 0.026 ± 0.00045 s^{-1}) (Fig. 1*B*).

We next determined the crystal structure of the RBBp4–SALL4(1–12 aa) complex to obtain structural information of the SALL4–RBBp4 protein–protein interaction site. The complex was solved at 2.7-Å resolution (*SI Appendix*, Table S1). RBBp4 forms a seven-sheet β-propeller (residue 33–404) with an N-terminal α-helix (Fig. 1*C*). All 12 residues of the SALL4 peptide are well defined in the electron density map, with 9 of the residues making favorable interactions with RBBp4. The substrate binding site of RBBp4 is highly acidic, with eight glutamic acid and two aspartic acid residues within 5 Å of the SALL4 peptide. This negatively charged interface binds the predominantly positively charged SALL4 peptide, which has five basic residues: Arg3, Arg4, Lys5, Lys8, and His11 (Fig. 1 *D* and *E*). Arg3 and Lys5 of SALL4 form charged interactions with Glu275, Glu319, and with Glu126, Glu179, respectively, in RBBp4 (Fig. 1*F* and *SI Appendix*, Table S2). Arg4 forms a salt bridge with Glu231, whereas His11 makes π–cation interactions with Trp42. Several unique hydrogen bonding contacts were observed between Arg3:Lys376, Arg4:Phe321, Arg4:Arg129, and Pro9:Ser73 of the RBBp4–SALL4 complex (Fig. 1*F* and *SI Appendix*, Table S2). Additional hydrogen bonds between residues Ser2 to Gln6 and Gln10 to Ile12 stabilize the SALL4 peptide, and several hydrophobic interactions stabilize the complex. The Arg4 side chain is deeply buried into RBBp4 (buried surface area 211 $Å^2$), whereas Lys5 and Pro9 bind in shallow grooves.

RRK Residues Are Crucial for RBBp4–SALL4 Interaction. Structural analysis of the RBBp4–SALL4(1–12) complex revealed a large

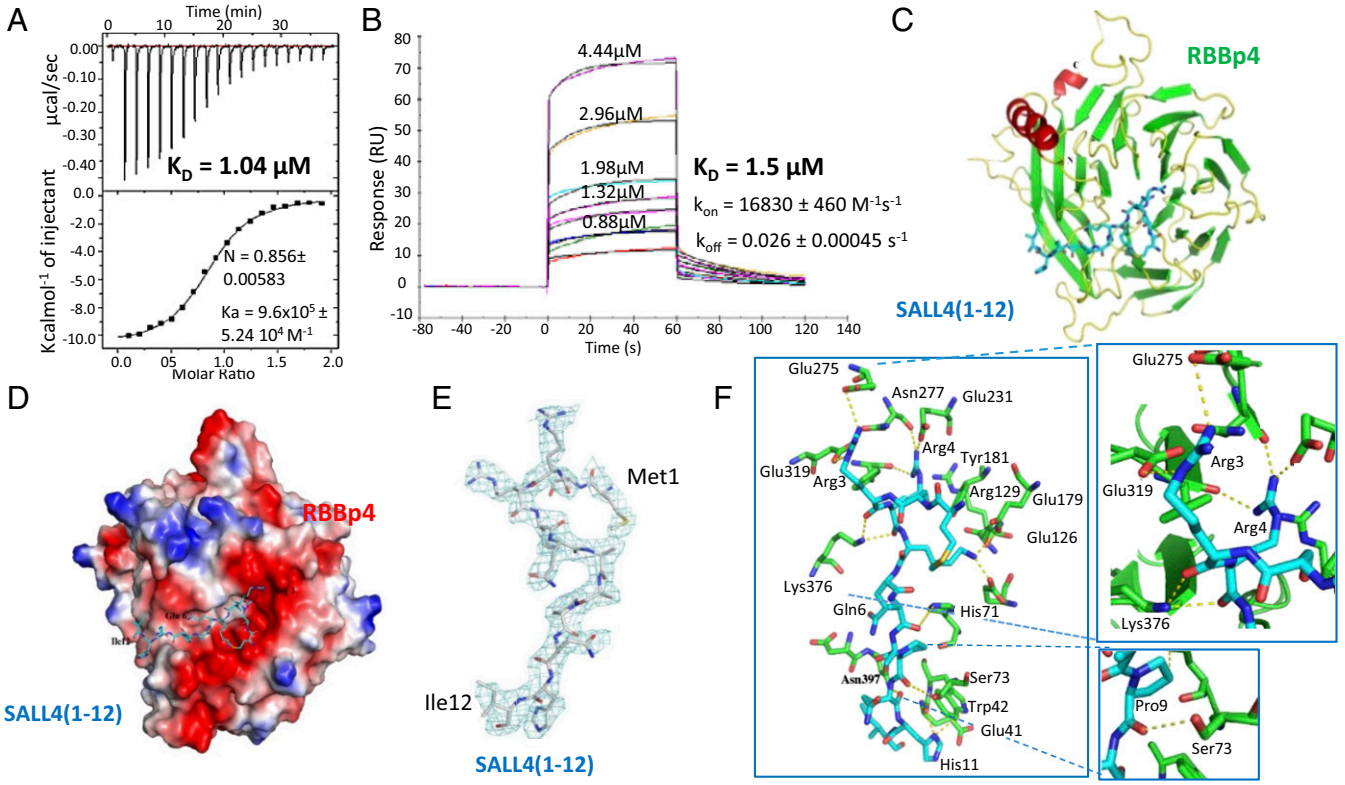

Fig. 1. Structure of RBBp4–SALL4(1–12) complex and their binding affinity. (*A*) ITC profiles of SALL4 WT peptide titrated against RBBp4 are shown in raw (*Upper*) and a simulated curve in a 1:1 binding model (*Lower*). (*B*) Sensorgram of SPR demonstrated binding of SALL4 WT peptide to RBBp4 immobilized on a dextran-coated chip. (*C*) Front view of the RBBp4–SALL4(1–12) complex. RBBp4 is depicted in yellow, green (β-sheet), and red (α-helix), and the SALL4 peptide is depicted in blue. N and C termini of RBBp4 are labeled. (*D*) Diagram representing electrostatic potential. Acidic patches are indicated in red, neutral in white, and basic in blue. (*E*) The final $2F_o–F_c$ electron density map (contoured at 1σ) for the key residues of SALL4 peptide from Met1 to Ile-12. (*F*) Side chains of RBBP4 (green) interacting with SALL4 peptide (blue) is shown in stick representation. Unique interactions of SALL4–RBBp4 are shown in the boxes.

and shallow acidic interaction surface, suitable for developing a peptide inhibitor to block the interaction. In this regard, we undertook an integrated approach by combining computational studies with biophysical assays to determine the important amino acids for the SALL4–RBBp4 interaction. The structural analysis of the complex indicated that Arg3, Arg4, and Lys5 of SALL4 are crucial for binding. We confirmed this structural hypothesis using computational alanine scanning, and found that alanine substitutions of Arg3, Arg4, and Lys5 greatly affected the binding free energy (19, 16, and 14 kcal/mol, respectively) (Fig. 2*A*). Based on the in silico analysis, we subsequently performed a biochemical alanine scan of these residues with a series of mutant peptides using a fluorescence polarization assay (Fig. 2 *B* and *C* and *SI Appendix*, Fig. S1). Compared with the WT peptide (IC_{50} = 1.0 μM), peptides bearing R3A, R4A, or K5A mutations demonstrated significantly decreased IC_{50} values (4.5, 8.9, and 7 μM, respectively) (Fig. 2*B*), whereas the Q6A mutation had a minimal effect (IC_{50} = 1.3 μM). Double mutations with two key residues, R3A,R4A; R4A,K5A; and R3A,K5A; abolished the interaction, with IC_{50} values noted above 100 μM, whereas double mutants with the loss of only one key residue showed reduced but positive binding (IC_{50} = 4.4 μM, 4.1 μM, and 4.7 μM, respectively) (Fig. 2*B* and *SI Appendix*, Fig. S1). These findings confirmed that Arg3, Arg4, and Lys5 are essential residues involved in the SALL4–RBBp4 interaction.

We next selected a representative double mutant of essential residues (MSARAQAKPQHI; MUT R3A,K5A) and compared its effect with the WT peptide on cell viability in SNU398 HCC cells, which express high levels of SALL4 RNA and protein (16). While the WT peptide exerted an inhibitory effect on cell number, the MUT peptide did not (Fig. 2*D*). Further qPCR analysis revealed a threefold increase in PTEN expression (P < 0.0001) in cells treated with the WT peptide compared with untreated cells, whereas MUT-treated cells again showed no significant change (P value not significant) (Fig. 2*E*). These findings indicate that the MUT peptide could not block the RBBp4–SALL4 interaction and failed to release the suppressive complex from the PTEN promoter, unlike its WT counterpart.

Optimization of a Candidate Therapeutic Peptide. After determining the key interactions between RBBp4 and SALL4(1–12), and by using structural data of the RBBp4–SALL4(1–12) complex as a platform, we then undertook a peptide substrate-based approach to design and optimize a potent inhibitor of the SALL4–RBBp4 interaction. We first determined the minimum length required for bioactivity through a truncation analysis of the WT peptide (*SI Appendix*, Table S3, peptide 1). Removing the first two N-terminal residues, Met and Ser (*SI Appendix*, Table S3, peptides 2 and 3), increased the peptide binding affinity to RBBp4 compared with the WT (IC_{50} = 0.60 and 0.36 vs. 1.0 μM, respectively); yet C-terminal truncations resulted in a marginal loss of binding affinity (*SI Appendix*, Table S3) (IC_{50} = 1.29, 0.80, and 1.91 μM for peptides 5, 6, and 7, respectively). Removal of a key binding residue (peptide 4) abolished the binding affinity (IC_{50} > 20 μM). To further improve binding potency, peptide 3 was selected as the sequence template and subjected to a systematic single-residue mutation analysis with alanine substitutions. Substituting the nonessential residues of peptide 3 with Ala (*SI Appendix*, Table S3, peptides 11–16) yielded more potent peptides, whereas substituting the essential residues of peptide 3 with Ala abolished binding (*SI Appendix*, Table S3, peptides 8–10). This suggests that nonessential residues of peptide 3 could be replaced with other amino acid residues for sequence optimization. Systematic substitution of the nonessential residues (*SI Appendix*, Table S3, peptide 20–45) revealed a marked reduction of IC_{50} upon replacement of Gln-4, Pro-7, and His-9 of peptide 3. Gln4 sits in a small binding pocket formed by Pro43, His71, and Glu395 of RBBp4, which is able to accommodate amino acid

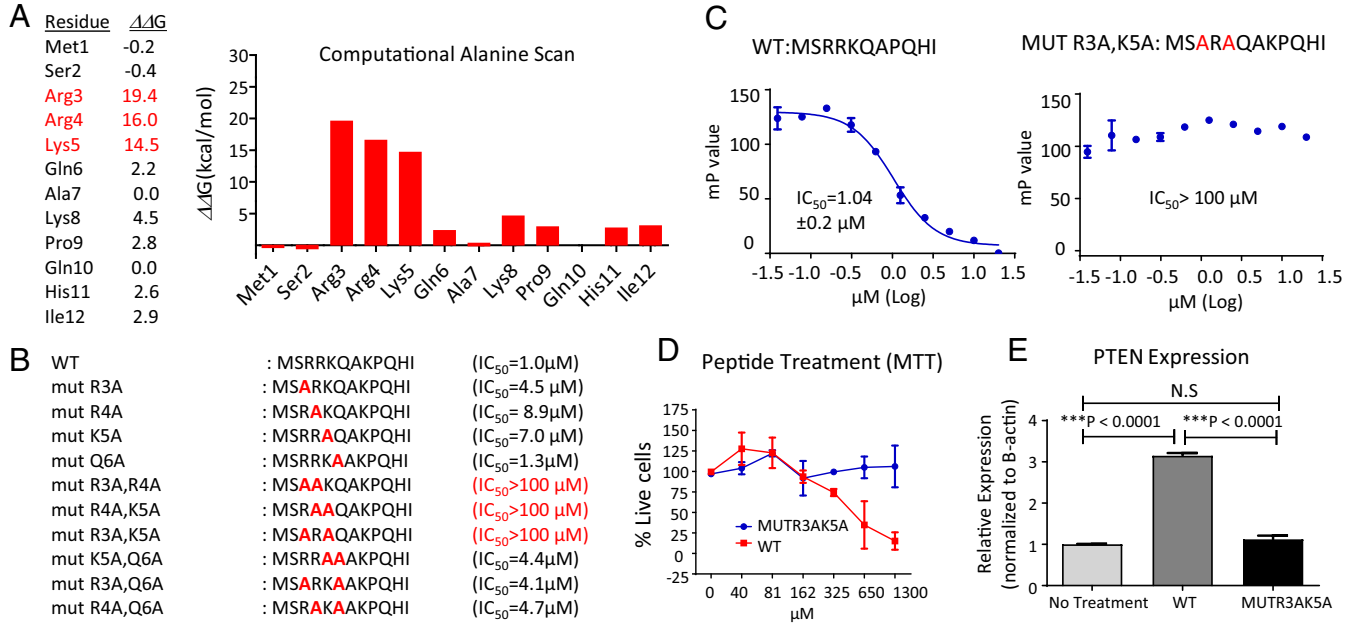

Fig. 2. Key residues involved in RBBp4–SALL4(1–12) binding. (*A*) Computational alanine scanning (CAS) was carried out on all 12 residues of the SALL4 peptide. The difference in the binding free energy ($\Delta\Delta G_{bind}$) of the alanine mutants (ΔG_{mutant}) and WT ($\Delta G_{wild\ type}$) was calculated ($\Delta\Delta G_{bind} = \Delta G_{mutant} - \Delta G_{wild\ type}$). $\Delta\Delta G_{bind}$ was tabulated (*Left*) and plotted in a bar chart (*Right*). (*B*) Alignment of mutant peptides. Mutated residues are highlighted in red. The IC_{50} of each peptide, including WT, was determined by fluorescence polarization. Different concentrations of each peptide were titrated into a mixture of 0.045 μM RBBp4 and 0.1 μM of C-labeled FITC-SALL4 WT peptide. Polarization was measured in millipolarization. (*C*) Representative IC_{50} curves of SALL4 WT and double-mutant MUT R3A,K5A by fluorescence polarization. (*D*) Cell viability assays were performed on SNU398 cells treated with SALL4 WT or MUT R3A,K5A peptides. Pep-1 carrier was added to the peptide to facilitate cellular penetration of the peptides. (*E*) Cells were treated with 8 mM of peptides with Pep-1 carrier for 24 h, and transcript levels of the SALL4–RBBp4 downstream gene, PTEN, were measured using quantitative real-time PCR. Data represent mean ± SD (n = 3). N.S., not significant.

residues with hydrophobic side chains. Consequently, substituting Gln4 with Leu or Phe (peptides 23 and 24) led to improved binding affinities, particularly Phe, which induced a sevenfold enhancement in binding affinity over that of peptide 3 (IC_{50} 0.05 vs. 0.36 μM) (*SI Appendix*, Table S3). Additionally, a Phe substitution (peptide 34) for Pro7 further increased the potency of the peptide (IC_{50} 0.17 vs. 0.36 μM) (*SI Appendix*, Table S3). Using computer modeling, the aromatic ring of Phe7 was found to be solvent-exposed and not involved in RBBp4 binding. However, its backbone amide proton could be involved in H-bonding to the side-chain carboxyl moiety of Glu395, an interaction lacking in Pro7 (*SI Appendix*, Fig. S2). In an effort to enhance the π–π interaction to RBBp4, His9 was replaced by aromatic residues Trp (peptide 41), and the substitution improved the binding affinity by threefold compared with that of peptide 3 (IC_{50} 0.12 vs. 0.36 μM) (*SI Appendix*, Table S3).

These three substitutions (Gln4Phe, Pro7Phe, and His9Trp) were incorporated into peptide 46 (RRKFAKFQWI, named FFW hereafter). Fluorescence polarization assay confirmed the high potency of FFW, with a >43-fold increase in affinity compared with the original 12-residue WT peptide (IC_{50} = 0.023 vs. 1.0 μM) (*SI Appendix*, Fig. S3 and Table S1).

FFW Reverse-Transcription Repression by SALL4–RBBp4. To elucidate the regulatory pathways that FFW could affect, a penetratin sequence (PEN) was attached to the N terminus of FFW to facilitate penetration into cells in culture (Fig. 3*A*). The FFW peptide is a highly basic and hydrophobic molecule. To test the ability of FFW to penetrate cells without the penetratin sequence, we treated both peptides to SNU398 cells and MTT assays were conducted after 72 h of incubation. The results demonstrated that although FFW is hydrophobic, the FFW peptide did not show any effect on cell viability without the conjugation of the penetratin sequence (Fig. 3*B*). We have also conjugated FITC to the amino terminus of FFW and subjected it to fluorescence microscopy, but could not detect any uptake of the peptide by the cells (*SI Appendix*, Fig. S4).

In addition to PEN-FFW, the PEN sequence was also conjugated to WT and MUT peptides. To test if the PEN-FFW peptide could disrupt endogenous SALL4–NuRD interaction, we performed coimmunoprecipitation after peptide treatment using SALL4 antibody (Fig. 3*C*). We found that the endogenous SALL4–RBBp4/HDAC/NuRD interaction was abrogated after PEN-FFW treatment, but not the controls. We next sequenced RNA transcripts (RNA-seq) from SNU398 cells treated with PEN alone, and different PEN conjugated peptides (30 μM, 8 h). Unbiased hierarchical clustering of the whole transcriptome data revealed that the PEN-FFW–treated sample was distinctly clustered away from the rest of the samples (Fig. 3*D*), whereas PEN- and PEN-MUT–treated samples (controls) were closely clustered together with similar transcriptome profiling, and the PEN-WT–treated sample was clustered in between. Strikingly,

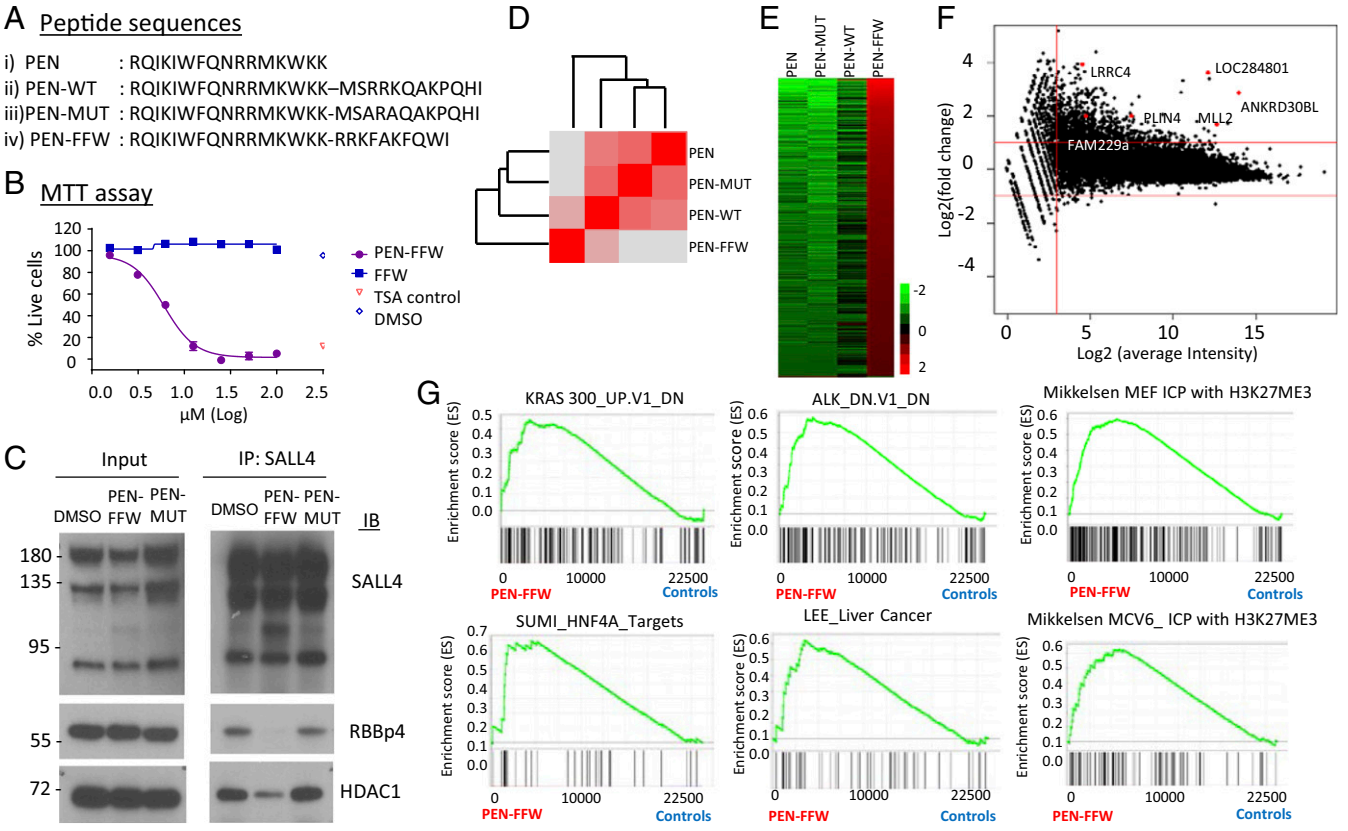

Fig. 3. Transcriptome profiling of the PEN-, PEN-MUT–, PEN-WT–, and PEN-FFW–treated SNU398 cells. (*A*) The penetratin sequence was added to WT, MUT, and FFW peptides to aid cellular penetration. (*B*) SNU398 were treated with FFW without the penetratin sequence (FFW), or FFW conjugated with the penetratin sequence (PEN-FFW), and subjected to a cell viability assay (MTT) after 72 h. TSA (Trichostatin A) was used as positive control. DMSO was included as vehicle control. (*C*) SALL4 was immunoprecipitated from SNU-398 nuclear extracts (1×10^6 cells) pretreated with DMSO, PEN-FFW (30 μM), or PEN-MUT (30 μM) for 4 h. Immunoprecipitates were analyzed by Western blot using SALL4, RBBp4, and HDAC1 antibodies. SALL4–RBBp4/NuRD interaction was abrogated by PEN-FFW treatment. (*D*) Hierarchical clustering based on whole transcriptome profiling, demonstrating that PEN-FFW distinctly clustered away from PEN, PEN-MUT, and PEN-WT. (*E*) Heatmap presentation of the DEGs encoding cell adhesion molecules, tumor suppressors, and apoptosis-related transcripts. (*F*) M-A (log-average fold-changes versus logarithmic mean intensity) plot of PEN-FFW over the control PEN demonstrating that significantly changed genes are almost all up-regulated. (*G*) GSEA in PEN-FFW versus the controls (PEN and PEN-MUT) using the whole transcriptome of the samples.

heatmap presentation of differentially expressed genes (DEGs) demonstrated that PEN-FFW treatment induced almost exclusively gene activation, in which 99.5% of the PEN-FFW DEGs were up-regulated (575 transcripts) and only 0.5% of the DEGs (three transcripts) were down-regulated (Fig. 3*E* and Dataset S1). This indicate that the PEN-FFW treatment had reversed the repressive function of SALL4, switching it from a dual-action transcription factor to a single-activator mode. This observation was further confirmed by M-A plot (log fold-change versus log mean intensity) of PEN-FFW versus controls (Fig. 3*F*), in which a majority of the DEGs are up-regulated.

Next, gene set enrichment analysis (GSEA) was performed using the whole transcriptome between PEN-FFW or PEN-WT and the two negative controls (PEN and PEN-MUT), respectively. GSEA analysis revealed a significant concordance between genes up-regulated in cells treated with PEN-FFW and genes down-regulated by overexpressing oncogenes like KRAS and ALK (Fig. 3*G* and Datasets S2 and S3). Genes down-regulated in HCC, for example *ATP1A2* and *LCN8*, were also specifically up-regulated in PEN-FFW–treated samples, while further analysis showed that targets of HNF4a, a key liver transcription factor, were also enriched in PEN-FFW–treated cells. Interestingly, PEN-FFW–enriched genes were associated with the repressive H3K27Me3 mark before peptide treatment, indicating these transcripts had undergone epigenetic modulation following disruption of the SALL4–NuRD interaction. (Fig. 3*G* and Dataset S3).

SALL4–RBBp4 Disruption Induced Apoptosis and Enhanced Cell Adhesion. Next, we conducted chromatin immunoprecipitation coupled with next-generation sequencing (ChIP-seq) on SNU398 cells to detect the SALL4 binding regions in the genome to compare with the PEN-FFW DEGs. Of the 7,883 SALL4 binding peaks, 60% are located at promoter regions, with H3K27Ac marks enriched around the SALL4 peaks (Fig. 4*A*). Interestingly, 57 of the 575 PEN-FFW DEGs have strong SALL4 binding peaks within 2 kb of the transcription start sites, suggesting that these transcripts are direct targets of the SALL4–RBBp4/NuRD interaction (Fig. 4*B*). Furthermore, we observed that chromatin remodelers and transcripts encoding molecules that facilitate transcription activation are among the highest expressed DEGs of these 57 transcripts (Fig. 4*C*). These include: *POLR2A*, the largest subunit of POLII; pre-mRNA splicing factor *SRRM2*; and chromatin remodeling protein *SRCAP*. Interestingly, both of the H3K4-specific methytransferases, *MLL2* and *SETD1B*, also demonstrate promoter occupancy by SALL4 (Fig. 4*D*) and up-regulation after SALL4–RBBp4/NuRD disruption, implying that the SALL4–RBBp4/NuRD complex strongly regulates chromatin status.

A significant proportion of the PEN-FFW DEGs are miRNA and noncoding RNAs (23% of the transcriptome). We focused on annotated transcripts and performed pathway analysis for these transcripts. Intracellular Ca^{2+} concentration is tightly regulated in cells. An unexpected finding of the pathway analysis revealed that a group of transcripts involved in calcium signaling, such as calmodulin (*CALML6*) and *GRIN1*, are up-regulated (Fig. 4*E*), suggesting that SALL4–RBBp4 disruption might induce a Ca^{2+} influx in PEN-FFW–treated cells. Because Ca^{2+} could act as a secondary messenger to activate apoptosis (23), we detected transcripts encoding molecules involved in the apoptosis pathway, such as *CARD14*, *RAPSN*, *CHRNG*, and *BCL2L14*, in the PEN-FFW DEGs. To further investigate the effect of these gene changes, three liver cancer cell lines with high expression of SALL4, SNU398, Huh7, and Hep3B (16) were treated with different peptides for 6 h (*SI Appendix*, Fig. S5) or 24 h (Fig. 4*F*). The cells were stained with propidium iodide (PI) and anti-Annexin V antibody to assess the apoptotic cell population by flow cytometry. After 24 h, PEN-FFW treatment significantly increased the apoptotic population (PI^+/Annexin V^+, Annexin V^+) from 16.6% in PEN control to 32.5% after PEN-FFW treatment in SNU398 (Fig. 4 *F*, *i*); from 14.3% in PEN control to 73.5% in PEN-FFW treated Huh7 cells (Fig. 4 *F*, *ii*); and from 13.5% in PEN control to 51.7% in PEN-FFW treated Hep3B cells (Fig. 4 *F*, *iii*), supporting previous data from transcriptome analysis.

Loss of cell–cell or cell–extracellular matrix (ECM) contact is often observed in cancer as transformed cells gain motility and invasiveness. In contrast, gain of cell–cell and cell–ECM contact could inhibit cancer cell growth and prevent metastasis. In our transcriptome analysis, the most distinct cellular pathway associated with PEN-FFW DEGs were transcripts encoding molecules involved in cell–cell adhesion and ECM interactions, including *CDH4*, *Claudin-5*, *-18*, and *-20*, collagen (*COL4A4*, *COL5A1*), integrin (*ITGA10*), laminin (*LAMA5*), and vitronectin (*VTN*). Furthermore, a group of cadherins were also up-regulated (*CDH4*, *FAT2*, *PCDH12*, *PCDHAG12*) after PEN-FFW treatment. We therefore hypothesize that the disruption of SALL4–RBBp4 could tighten cell–cell contacts and limit mobility of these cells. To examine this hypothesis, we performed a cell-invasion assay in Boyden chambers in which serum-starved SNU398, Huh7, or Hep3B cells were treated with different peptides (10 μM). Cells migrating toward 10% serum and invading the membrane pores after 24 h were stained with DAPI, and quantified by counting cells per microscope field-of-view. Compared with PEN- and PEN-MUT–treated cells, cell migration ability was indeed markedly impaired in PEN-FFW–treated cells. For both SNU398 and Huh7, more than an 85% reduction of migrated cells was observed in the PEN-FFW–treated group, compared with PEN (Fig. 4*G*) ($P < 0.001$ and $P < 0.0001$, respectively). For Hep3B, the migration activity is low compared with the other two cell lines, in which only 44 cells were found to have passed the membrane after PEN treatment, and this number dwindled to 14 cells after PEN-FFW treatment. Wound-healing assays were also performed to assess the migration activity of PEN-FFW–treated cells. We found that PEN-FFW–treated cells had slower migration activity compared with PEN-MUT and PEN controls in SNU398 (Fig. 4*H*), Huh7, and Hep3B cells (*SI Appendix*, Fig. S6).

Beside the pathways mentioned previously, a class of tumor suppressor genes was also restored after PEN-FFW treatment (Fig. 4*E*). *TSC1/2*, which inhibits mTORC1 (24), was enriched 2.5-fold after PEN-FFW treatment (Dataset S1). Another example, *LRRC4*, which functions to delay cell cycle progression (25), was increased after PEN-FFW treatment. A negative regulator of RAS, *DOK3*, was also found up-regulated in the PEN-FFW treated cells. Taken together, our data suggest that the disruption of the SALL4–RBBp4 interaction by the PEN-FFW peptide could lead to up-regulation of cell adhesion molecules to suppress migration, Ca^{2+} influx to induce apoptosis, and a group of tumor suppressors that oppose various oncogenic processes.

Prognostic Value of PEN-FFW Up-Regulated Genes. Because PEN-FFW treatment leads to significant apoptosis of SNU398 liver cancer cells (Fig. 4*F*) and dramatic inhibition of xenograft tumor growth (as presented below; see also Fig. 6), we were interested in evaluating the potential prognostic value of these PEN-FFW up-regulated DEGs in patients. Thus, we first overlapped these up-regulated genes with genes that are significantly up-regulated in normal liver samples compared with liver cancer patients in three independent cohorts (Fig. 5*A*, schematic representative of the analysis). Across the three cohorts, 26 of these PEN-FFW up-regulated DEGs show consistent overexpression in adjacent nontumor samples compared with the tumor (Fig. 5*B* and Dataset S4). We next explored their diagnostic abilities in separating HCC samples from normal tissues using the receiver operator curve (ROC), and were able to identify nine of them with consistently high area under curve across all three cohorts (Dataset S5). Three examples of these genes (IGFALS, GNAO1, and ECM1) are depicted in Fig. 5*C*.

Concomitantly, to further evaluate the prognostic relevance of these 26 PEN-FFW up-regulated DEGs, we examined their survival differences in two independent HCC cohorts. We were able to identify eight genes with favorable survival difference for the patients with high expression compared with those with low

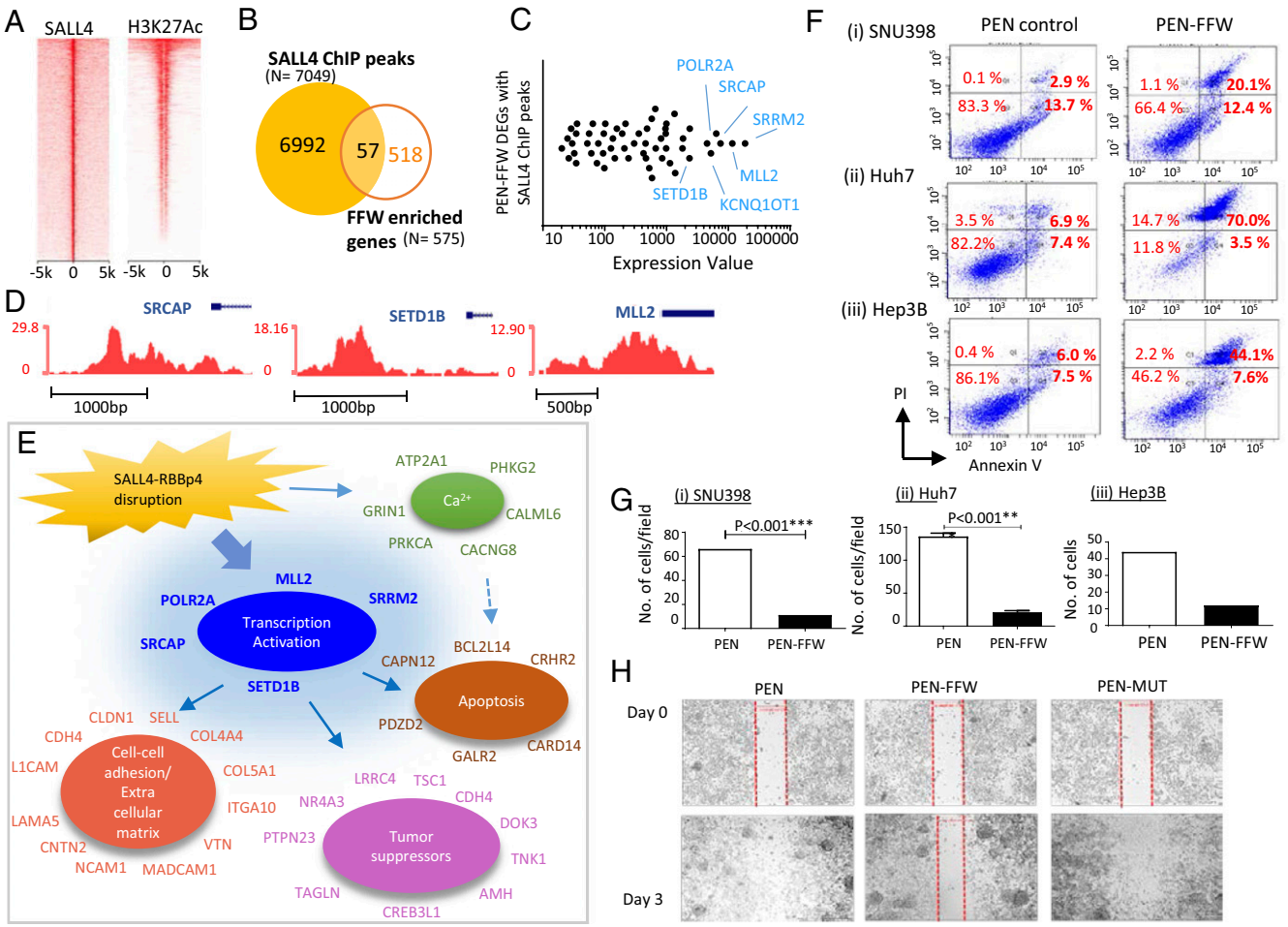

Fig. 4. Enhanced apoptosis and cell–cell adhesion by PEN-FFW treatment. (*A*) Heatmap representing the occupancy of SALL4 in the human genome. SALL4 binding loci were enclosed by histones marked with H3K27Ac. The number indicates fold-change after scaling the ChIP-seq signal to 1× coverage of the genome. (*B*) Venn diagram showing the overlap between the SALL4A ChIP-seq peaks and PEN-FFW DEGs in SNU398 cells. (*C*) RNA expression value of the 57 overlapped transcripts showed a group of transcription modelers were highly enriched. (*D*) Genome browser tracks of the ChIP-Seq representing the occupancy of SALL4 at three representative promoters. (*E*) Gene Ontology analysis revealed pathways altered in the PEN-FFW–treated cells under the control of SALL4–NuRD. (*F*) Annexin V/PI apoptosis assay were performed with PEN- (30 μM) and PEN-FFW– (30 μM) treated (*i*) SNU398, (*ii*) Huh7, and (*iii*) Hep3B cells, after 24 h of peptide incubation. Apoptotic populations were accessed by flow cytometry and from Annexin V^+ quadrants. (*G*) Transwell migration assay using PEN- (1 0 μM) and PEN-FFW– (10 μM) treated SNU398, Huh7, and Hep3B cells. (*H*) Wound-healing assay using SNU398 cells after low concentration (10 μM) treatment of different peptides for 3 d. Images of the cells were captured on day 0 and day 3 after peptide treatment. On day 0, the clear space created by the scratch was marked with red dotted vertical lines. On day 3, any remaining clear space was marked by the red dotted vertical lines, with no marking if the space was fully invaded by adjacent cells.

expression (Fig. 5*A* and Dataset S6). By overlapping the two gene sets from ROC and survival analysis, we were able to identify four PEN-FFW up-regulated DEGs having both high diagnostic and high prognostic values, and they are IGFALS, SLC22A1, ASPG, and FTCD. The favorable survival difference from these four genes is depicted in Fig. 5*D*, using two independent cohorts. The prognostic value and diagnostic value of these four genes are highlighted in bold in Datasets S5 and S6.

Therapeutic Peptide FFW Leads to Tumor Regression in Xenograft Models. Having developed the highly potent FFW peptide affecting SALL4 transcription, we next compared its efficacy to WT and mutant peptides at the cellular level. SNU398 cells were treated with PEN-MUT, PEN-WT, and PEN-FFW for 72 h with a series of concentrations, and cell viability was measured with the MTT assay. We observed that PEN-FFW conferred a 4-fold improvement in reducing cell viability compared with the PEN-WT (Fig. 6*A*) (EC_{50} 7.6 μM vs. 30 μM, respectively), and more than 13-fold compared with PEN-MUT (EC_{50} > 100 μM). To further confirm the specific therapeutic effect of PEN-FFW in SALL4-expressing HCC cells, we employed SNU398, Huh7, and Hep3B, three HCC lines with high levels of SALL4 (16); SNU387, a HCC line with undetectable levels of SALL4; and THLE-2 and THLE-3, immortalized normal liver epithelial cell lines with undetectable levels of SALL4, and treated these cells with PEN-MUT, PEN-WT, or PEN-FFW peptides (*SI Appendix*, Fig. S7). Our data demonstrate the specificity of PEN-FFW in targeting SALL4-high HCC cells (SNU398, Huh7, and Hep3B), and not SALL4-low HCC cells (SNU387) or immortalized normal liver epithelial cell lines THLE-2 and THLE-3, highlighting a clear therapeutic window for treatment.

To further test the therapeutic effect of PEN-FFW in vivo, SNU398 cells were implanted subcutaneously into the flanks of NOD/SCID/γ-mice (NSG), and the mice were randomly grouped for peptide treatments (n = 5 per group) (Fig. 6*B*). For mice treated with PEN (control) or PEN-MUT, tumors progressively increased in size, showing that neither peptide was able to inhibit tumor growth (Fig. 6*C*). In contrast, although PEN-WT impaired tumor growth (P = 0.001), PEN-FFW induced a much stronger therapeutic effect (P = 0.0008) with a tumor growth inhibition of

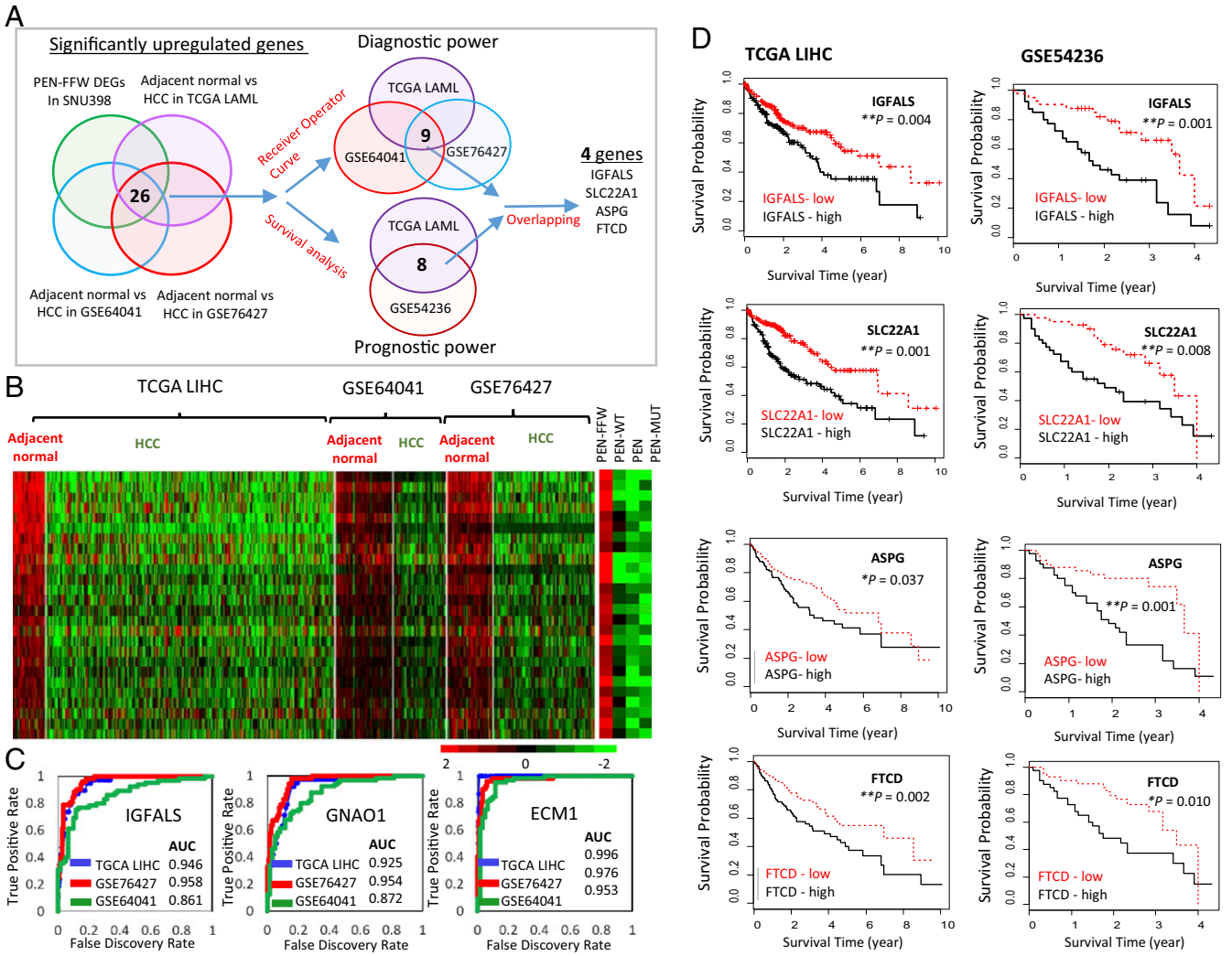

Fig. 5. PEN-FFW DEGs predicted favorable outcome for HCC patients. (*A*) Schematic representation of the integrated analysis of treatment data with patient data for selection of PEN-FFW up-regulated genes having both diagnostic and prognostic values. (*B*) Heatmap showing 26 genes with consistent up-regulation in adjacent nontumor tissue compared with liver tumor samples across three independent cohorts (TCGA-LIHC, GSE64041, and GSE76427). (*C*) ROC performance of three genes (IGFALS, GNAO1, and ECM1) as examples for the further selection of the 26 genes for separation of tumor samples from adjacent nontumor tissue across three independent cohorts. (*D*) Kaplan–Meier analysis of IGFALS, SLC22A1, ASPG, and FTCD in further selection of the 26 genes for favorable survival across two independent cohorts (TCGA-LIHC, *Right*; GSE54236, *Left*).

85%. PEN-FFW–treated mice also displayed the smallest tumors (Fig. 6*D*), with significantly lower tumor weight (μ = 88 mg in PEN-FFW, μ = 564 mg in PEN-WT, and μ = 1,550 mg in PEN control) (Fig. 6*E*). To access toxicity, we tabulated the body weight of the mice at end point (*SI Appendix*, Fig. S8) and also traced the body weight change throughout the experiment, and found no significant difference, suggesting the overall well-being of the mice receiving the peptide treatments.

To benchmark against current therapy used in advanced stage HCC, we compared PEN-FFW–treated SNU398 tumor xenografts to that of Sorafenib-treated xenografts in a separate set of experiments (*SI Appendix*, Fig. S9) (n = 6 per treatment group). Interestingly, PEN-FFW treatment resulted in stronger antitumor activity than Sorafenib compared with vehicle-treated groups, albeit not statistically significant. Furthermore, mice treated with PEN-FFW in combination with Sorafenib showed the slowest rate of tumor growth. These data suggest a potential therapeutic effect of PEN-FFW in treating HCC patients, including those refractory to Sorafenib treatment. To further test this hypothesis, we developed a second xenograft model with a chemo-resistant HCC cell line, PLC8024, which is both SALL4$^+$ and CD133$^+$, and also radioresistant (26, 27) (n = 6 per treatment group). In this chemoresistant model, we observed greater tumor growth (+1.5-fold) in the Sorafenib-treated group compared with the vehicle control group (Fig. 6*F*). Although PEN-FFW treatment showed minimal tumor inhibitory effect in this model, a significant synergistic effect of Sorafenib and PEN-FFW was observed in mice treated with both agents (P = 0.02, tumor growth inhibition 57% and 73% compared with control and sorafenib treated group, respectively) (Fig. 6*F*). This result further suggests that PEN-FFW alone, or as part of combination therapy, could bring clinical benefits to advanced stage HCC patients to overcome resistance to Sorafenib.

Drug-Like Properties of FFW. Biologics or compounds rapidly degraded in plasma generally demonstrate little efficacy in vivo. To further evaluate the potential of further development of PEN-FFW as a drug candidate, we examined the plasma stability, cell-penetration kinetics, and toxicity of the peptide. First, we monitored the degradation of PEN-FFW (1 μM) in de-identified, healthy human plasma by LC-MS/MS. At 30-min incubation (Fig. 7*A*, *Inset*), more than 90% of the peptide remained in the plasma. In comparison, the compound Eucatropine as a control was

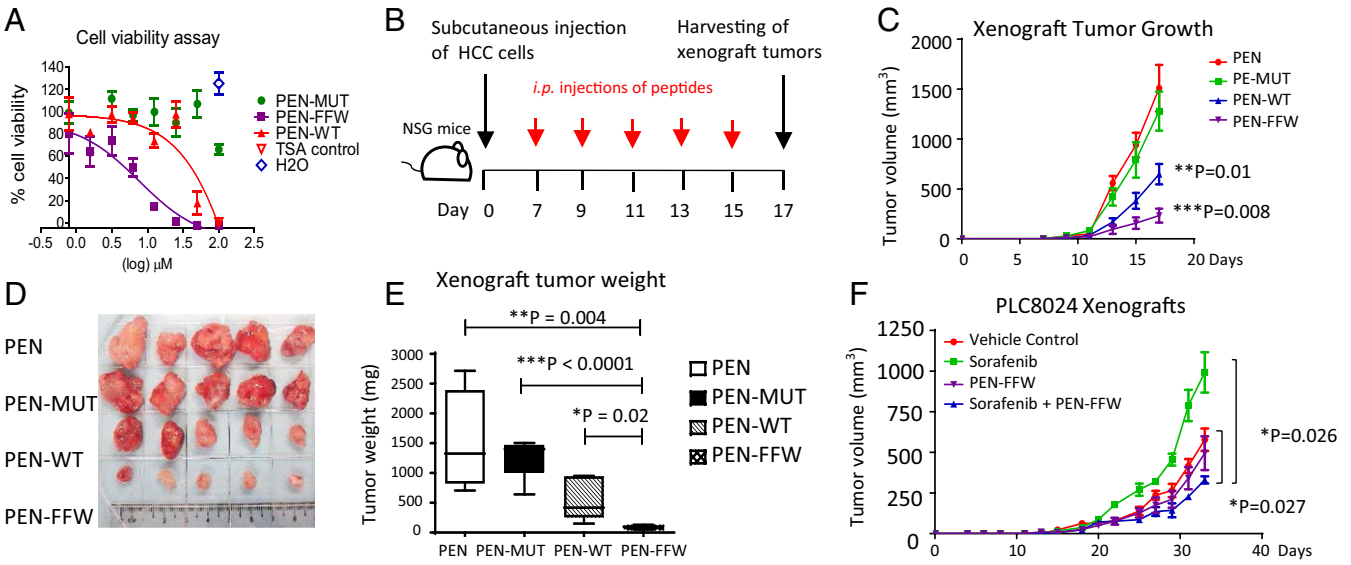

Fig. 6. Antitumor activity of the candidate therapeutic peptide FFW. (*A*) Penetratin-conjugated peptides were subjected to the cell viability assay in SNU398 cells, demonstrating the high potency of PEN-FFW. TSA (Trichostatin A) was used as positive control to reduce cell viability. (*B*) 7.2×10^5 SNU398 cells were inoculated subcutaneously into the right flank of NSG mice. Tumors grew for 1 wk before peptide treatment was administered on alternate days for a total of five injections. (*C*) Tumor growth was observed and charted using tumor volume vs. time. Data represent mean ± SD ($n = 5$). (*D*) Relative tumor size on day 17. (*E*) Tumor weight of mice from *C* ($n = 5$ per group): PEN-FFW, μ = 88.34 mg; PEN, 1,550.78 mg; PEN-MUT, 1,273.46 mg; PEN-WT, 563.46 mg. Data represent mean ± SD ($n = 5$). The experiments were performed twice independently; representative data from a single experiment are shown. (*F*) NSG mice were inoculated with 1×10^6 PLC8024 cells. Vehicle control, Sorafenib (20 mg/kg), PEN-FFW (30 mg/kg), and combination of Sorafenib (20 mg/kg) and PEN-FFW (30 mg/kg) were administered when xenografts reached 70–100 mm^3 ($n = 6$ per group). Tumor growth was observed and charted using tumor volume vs. time. The experiments were performed twice independently; representative data from a single experiment are shown.

rapidly degraded to 40% (*SI Appendix*, Fig. S10, *Inset*). Extending the experiment duration by 24 h revealed more than 50% of the peptide remained intact in the plasma after 4 h, gradually decreasing to ∼20% on the 24th hour (Fig. 7*A*). This suggests that PEN-FFW can potentially be developed as an intravenous drug. We subsequently conjugated FITC to the N terminus of PEN-FFW to assess the permeability and stability of the peptide in cells. Live cell imaging was performed on the treated cells at 2-min intervals for the first hour, and at 5-min intervals for the subsequent 23 h. It was observed that FITC-PEN-FFW entered cells by 18 min, and translocated to the nucleus by 22 min. At 2.5 h, FITC-PEN-FFW had entered every cell in the microscopic field, with incremental FITC-signals at 24 h (Fig. 7*B* and Movie S1).

Finally, potential toxic effects of the peptide were assessed with C57BL/6 mice harboring an intact immune system ($n = 4$). The mice were exposed to intraperitoneal administration of PEN-FFW (30 mg/kg) or vehicle (10% DMSO) every alternate day over the course of 17 d to a cumulative dose of 270 mg/kg. Mice in both groups remained alert, responsive, and did not exhibit notable signs of toxicity, such as lethargy, loss of mobility, or weight loss (Fig. 7*C*). After a 7-d washout period, complete blood counts and liver-function assay tests were performed, and organs were harvested for histology. To access potential liver injury caused by the peptide treatment, serum AST (aspartate aminotransferase) and ALT (alanine aminotransferase) levels were tested. Elevation of the two enzymes was not observed in the treatment group (Fig. 7*D*), indicating no liver damage was detected following treatment. Concurrently, no significant change in blood counts (Fig. 7*E*) or tissue damage (Fig. 7*F*) was observed in the treatment group compared with the control group.

Discussion

HCC is a deadly disease that lacks treatment options and alternative therapeutic approaches are urgently needed. In this report, we present our strategy to target HCC. We have previously found that SALL4 is elevated in a subclass of HCC enriched with hepatic progenitor cell features (16), and patients with this subtype suffer from a poor prognosis. RBBp4 is an essential subunit of NuRD complex, which in turn plays a key role in maintaining silencing of key regulators during embryonic development. A deregulated SALL4–RBBp4/NuRD pathway results in silencing of tumor suppressors, such as PTEN in HCC cells. Therefore, targeting the SALL4–NuRD pathway in HCC is a promising therapeutic approach. To further understand the mechanism of interaction, we first determined the crystal structure of the RBBp4–SALL4(1–12) complex. The crystal structure revealed a large, acidic interaction surface between the two nuclear factors, with side chains of the SALL4(1–12) peptide intercalating into the grooves of RBBp4, providing an opportunity for an engineered peptide to competitively inhibit the interaction (Fig. 8*A*). An integrated approach combining computational analysis, rational truncation, and systematic substitution studies was undertaken to design the therapeutic peptide. This approach facilitated the testing of peptide affinity down to single amino acid resolution, and provided real-time data feedback to the modeling, enabling further sequence enhancement. Using this approach, we were able to develop a potent SALL4–RBBp4/NuRD inhibitor that inhibits tumor growth in xenograft mouse models, targeting the "undruggable" nuclear factor.

Remarkably, the disruption of SALL4–RBBp4 with the FFW therapeutic peptide resulted in massive up-regulation of transcripts, which is very different from previous reports in which SALL4 was knocked down (16). SALL4 can both repress and activate genes, and down-regulation of SALL4 leads to both up- and down-regulation of its target genes. In contrast, within the observed time period, FFW peptide treatment caused a unidirectional transcription activity shift toward only up-regulation of target genes (Fig. 8*B*). We hypothesize that in cancer cells, reactivation of SALL4 causes repression of tumor suppressors and epithelial markers like cadherins, resulting in a progenitor-like, undifferentiated cancer cell type. Upon peptide disruption of the SALL4–RBBp4 axis, the repression of SALL4 function is released and results in mass activation of transcripts unfavorable for cancer cell survival but beneficial to patient survival.

In the transwell cell migration assay, it was demonstrated that PEN-FFW–treated cells have impaired cell migration compared

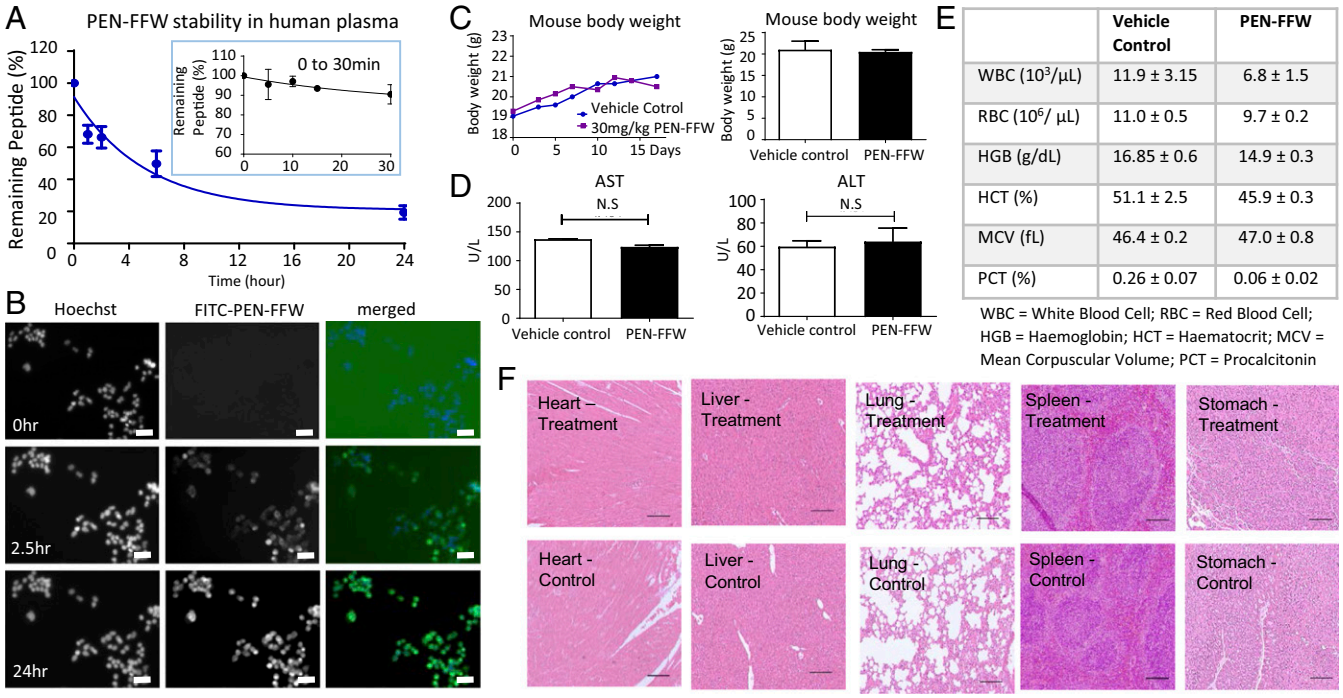

	Vehicle Control	PEN-FFW
WBC (10^3/μL)	11.9 ± 3.15	6.8 ± 1.5
RBC (10^6/ μL)	11.0 ± 0.5	9.7 ± 0.2
HGB (g/dL)	16.85 ± 0.6	14.9 ± 0.3
HCT (%)	51.1 ± 2.5	45.9 ± 0.3
MCV (fL)	46.4 ± 0.2	47.0 ± 0.8
PCT (%)	0.26 ± 0.07	0.06 ± 0.02

WBC = White Blood Cell; RBC = Red Blood Cell; HGB = Haemoglobin; HCT = Haematocrit; MCV = Mean Corpuscular Volume; PCT = Procalcitonin

Fig. 7. Drug-like properties of PEN-FFW. (*A*) The PEN-FFW peptide was incubated with human plasma to test for stability. Samples were subjected to LC-MS/MS measurement at 0, 5, 10, 15, and 30 min (*Inset*); and subsequently at 0, 1, 2, 4, and 24 h. (*B*) SNU398 cells were labeled with Hoechst 33342 for 5 min, and FITC-PEN-FFW was added to the media at 10 μM. Live cell imaging was performed with images taken at every 2 min for the first hour, and at 5-min intervals for the subsequent 23 h. Montages at 0, 2.5, and 24 h are shown. (Scale bars, 5 μm.) (*C*) Four C57BL/6 mice were exposed to vehicle or peptide treatment every alternate day for a total of 17 d. Serial body weights and end-point body weights of the mice are shown. (*D*) Serum AST and ALT of the mice were measured after a 10-d wash-out period after peptide treatment. No significant change between the two groups was observed. N.S., not significant. (*E*) Blood counts of the mice were performed at end point. (*F*) Representative microphotographs from the major organs (heart, liver, lung, spleen, stomach) harvested from vehicle control and PEN-FFW–treated animals are shown. The tissue sections were examined by a qualified pathologist. (Scale bars, 200 μm.)

with controls, and this phenotypic change corresponds to the up-regulation of transcripts encoding cell adhesion molecules and cadherins. Similar to knocking down SALL4, the disruption of SALL4–RBBp4 resulted in apoptosis (16). Together with the up-regulation of tumor-suppressor transcripts, the overall transcriptome change brought by FFW is at a disadvantage to tumor progression. Simultaneously, these transcripts are associated with a good prognosis in HCC patients, as shown by survival analysis.

The use of peptides as drugs may hold significant advantages over small molecules in targeting of protein–protein interactions, as large binding surfaces typically lack defined or deep binding pockets (28, 29). Thus, we chose to target the SALL4–RBBp4 protein–protein interactions using a peptide due to the large and predominantly shallow binding interface between SALL4 and RBBp4. Moreover, a well-designed peptide drug tends to possess higher selectivity with a safer toxicity profile compared with small molecules. In certain therapeutic areas in which small molecules have limited success, peptides have been shown to be valuable substitutes. For example, the development of protease-resistant stapled peptides with cell-penetrating capabilities (30) and new peptide formulations that enhance their oral bioavailability (31) have resulted in a dozen peptides in clinical trials and tens of approved peptide drugs (29). We tested the stability of PEN-FFW

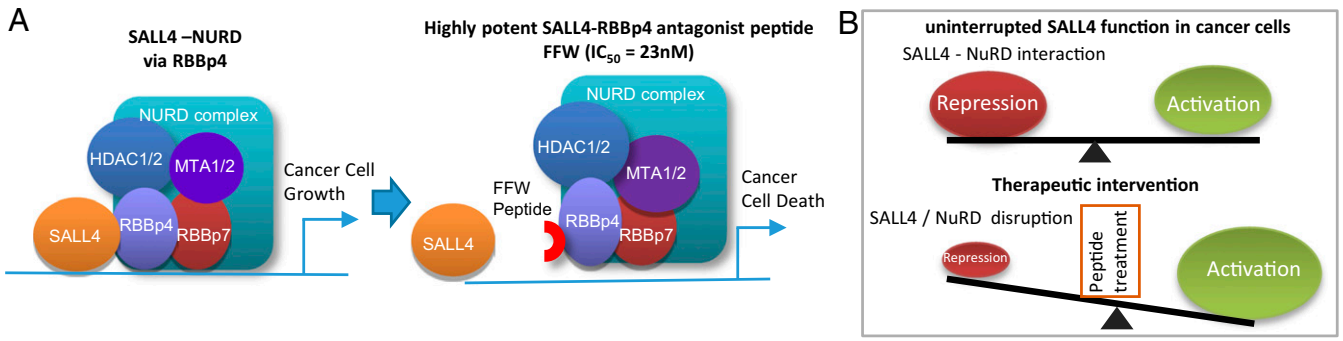

Fig. 8. Working hypothesis and model of SALL4 inhibition in cancer cells. (*A*) Model depicting the recruitment of the NuRD complex by SALL4 to the promoter of tumor suppressors, via binding to the RBBp4 subunit. The introduction of a FFW inhibitor abolishes the binding of SALL4 to RBBp4 and NuRD, and tumor suppressors are released from repression. (*B*) A model of SALL4's transcription activity in cancer cells, with both activation and repression of transcription activity balanced to promote cell survival. Upon therapeutic intervention with the FFW peptide, balance is interrupted and the repression activity of SALL4 is therefore lost, which in turn results in cancer cell death.

in human plasma, and the results demonstrated notable stability in which 90% of the peptide was retained after 30-min incubation under physiological conditions, gradually decreasing over time with 20% still intact at 24 h. This stability profile indicates a possibility to develop an intravenous delivery route for FFW. One advantage of using peptides as drugs is minimal toxicity. The suitability of further developing FFW is further supported by the low toxicity profile of FFW in C57BL/6 mice.

PEN-FFW is a specific SALL4–RBBp4/NuRD inhibitory peptide targeting SALL4$^+$ HCC by binding to RBBp4. This represents a first attempt to target RBBp4, a chaperone protein with WD40-repeats. In the nucleus, the RBBp4/NuRD complex binds to a few other lineage-specific proteins, such as BCL11B and FOG1. Several crystal structures of RBBp4 with its binding partners have been reported previously, including BCL11A (32), FOG-1 (33), and PHF6 (34). However, in the context of HCC cells, these molecules are not present or are expressed at very low abundance. Hence, we hypothesize that RBBp4/NuRD binds to different molecules in a cell-type–specific manner, and with this, the PEN-FFW peptide is specific to SALL4–RBBp4 binding in HCC cells.

A deregulated SALL4–RBBp4/NuRD pathway results in silencing of tumor suppressors in HCC cells. The SALL4–RBBp4/NuRD interaction represents an exciting target in HCC, and unlike HDAC inhibitors, which target cells nonselectively, this SALL4–RBBp4/NuRD interaction has been observed to be exclusive to cancer cells that express SALL4. It is worth mentioning that RBBp4 is present in other nuclear complexes, such as PRC2, MLL2, and Sin 3, functioning as a chaperone. It is possible that blocking RBBp4 could disrupt the formation of these general nuclear complexes in a cell-type–independent manner. Further investigations will need to be carried out to understand how the peptide would affect these complexes.

Through resolving the structure of the RBBp4–SALL4(1–12) complex, identification of the key interacting residues, and systematic peptide studies, a potent therapeutic peptide, FFW, was demonstrated to confer robust proapoptotic and antimigration effects in SALL4-expressing HCC cells, and induced marked improvement in therapeutic efficacy in mice bearing hepatocellular carcinoma tumors. Mechanistically, global genomic studies revealed that this FFW could convert SALL4 from a dual-regulator to an activator-only status. Overall, the FFW peptide could be the basis for development of a first-in-class drug, as there is currently no available inhibitor targeting the SALL4–RBBp4/NuRD interaction, and in addition, provide a viable therapeutic strategy for the significant subset of patients with HCC and many other cancers whose malignancies are driven by SALL4 expression.

Methods

Crystallization screens were performed with the hanging-drop vapor-diffusion method using Hampton Research screens. The RBBP4 protein was purchased from SinoBiological and concentrated to 8 mg/mL in 50 mM Tris 100 mM NaCl. The concentrated RBBP4 protein was mixed with 20 mM of SALL4 peptide and crystallization drops were set up at a 1:1 ratio. Diffraction quality crystals of SALL4(1–12) –RBBp4 complexes were obtained from a reservoir solution containing 0.2 M sodium chloride, 0.1 M Bis-Tris, pH 5.5, 25% PEG 3,350. Detailed protocol of crystallization and structure determination can be found in *SI Appendix, SI Material and Method*.

Detailed protocols for ITC, SPR, flourescence polarization, computational alanine scanning, cell culture and treatment with peptide, coimmunoprecipitation, migration and wound-healing assay, xenograft studies, plasma stability assay, live cell imaging, RNA-seq data analysis, ChIP, and ChIP-seq analysis can also be found in *SI Appendix, SI Material and Method*. All animal studies were conducted with the approval of the Institutional Animal Care and Use Committee (IACUC) of the National University of Singapore.

ACKNOWLEDGMENTS. The authors thank Dr. Supriya Srivastava for pathologic evaluation of the animal tissue sections and Dr. Chen-Lang Mok for editorial assistance. This research is supported by the Singapore Ministry of Health's National Medical Research Council under its Singapore Translational Research Investigator Award, and by the National Research Foundation Singapore and the Singapore Ministry of Education under its Research Centres of Excellence initiative. J.S. received funding from Singapore Ministry of Education–Tier-2 Grant WBS R154000625112 in support of this project. C.S.B.C., A.P., A.W.H., X.K.-S., J.H. and J.J. thank the A*STAR Biomedical Research Council for funding. L.C. was supported by NIH Grant PO1HL095489 and a research fund from the Leukemia and Lymphoma Society.

1. Lim CY, et al. (2008) Sall4 regulates distinct transcription circuitries in different blastocyst-derived stem cell lineages. *Cell Stem Cell* 3:543–554.
2. Yang J, et al. (2008) Genome-wide analysis reveals Sall4 to be a major regulator of pluripotency in murine-embryonic stem cells. *Proc Natl Acad Sci USA* 105:19756–19761.
3. Zhang J, et al. (2006) Sall4 modulates embryonic stem cell pluripotency and early embryonic development by the transcriptional regulation of Pou5f1. *Nat Cell Biol* 8:1114–1123.
4. Forghanifard MM, et al. (2013) Role of SALL4 in the progression and metastasis of colorectal cancer. *J Biomed Sci* 20:6.
5. Fujimoto M, et al. (2014) SALL4 immunohistochemistry in non-small-cell lung carcinomas. *Histopathology* 64:309–311.
6. Itou J, Matsumoto Y, Yoshikawa K, Toi M (2013) Sal-like 4 (SALL4) suppresses CDH1 expression and maintains cell dispersion in basal-like breast cancer. *FEBS Lett* 587:3115–3121.
7. Murakami T, et al. (2016) Clinicopathologic and immunohistochemical characteristics of gastric adenocarcinoma with enteroblastic differentiation: A study of 29 cases. *Gastric Cancer* 19:498–507.
8. Gao C, Kong NR, Chai L (2011) The role of stem cell factor SALL4 in leukemogenesis. *Crit Rev Oncog* 16:117–127.
9. Li A, et al. (2013) A SALL4/MLL/HOXA9 pathway in murine and human myeloid leukemogenesis. *J Clin Invest* 123:4195–4207.
10. Ma Y, et al. (2006) SALL4, a novel oncogene, is constitutively expressed in human acute myeloid leukemia (AML) and induces AML in transgenic mice. *Blood* 108:2726–2735.
11. Yang J, et al. (2007) Bmi-1 is a target gene for SALL4 in hematopoietic and leukemic cells. *Proc Natl Acad Sci USA* 104:10494–10499.
12. Ardalan Khales S, et al. (2015) SALL4 as a new biomarker for early colorectal cancers. *J Cancer Res Clin Oncol* 141:229–235.
13. Deng G, et al. (2015) SALL4 is a novel therapeutic target in intrahepatic cholangiocarcinoma. *Oncotarget* 6:27416–27426.
14. Han SX, et al. (2014) Serum SALL4 is a novel prognosis biomarker with tumor recurrence and poor survival of patients in hepatocellular carcinoma. *J Immunol Res* 2014:262385.
15. Miller A, et al. (2016) Sall4 controls differentiation of pluripotent cells independently of the nucleosome remodelling and deacetylation (NuRD) complex. *Development* 143:3074–3084.
16. Yong KJ, et al. (2013) Oncofetal gene SALL4 in aggressive hepatocellular carcinoma. *N Engl J Med* 368:2266–2276.
17. Zeng SS, et al. (2014) The transcription factor SALL4 regulates stemness of EpCAM-positive hepatocellular carcinoma. *J Hepatol* 60:127–134.
18. Gao C, et al. (2013) Targeting transcription factor SALL4 in acute myeloid leukemia by interrupting its interaction with an epigenetic complex. *Blood* 121:1413–1421.
19. Hainer SJ, Fazzio TG (2015) Regulation of nucleosome architecture and factor binding revealed by nuclease footprinting of the ESC genome. *Cell Rep* 13:61–69.
20. Harikumar A, Meshorer E (2015) Chromatin remodeling and bivalent histone modifications in embryonic stem cells. *EMBO Rep* 16:1609–1619.
21. Zhang W, et al. (2013) Structural plasticity of histones H3-H4 facilitates their allosteric exchange between RbAp48 and ASF1. *Nat Struct Mol Biol* 20:29–35.
22. El-Serag HB (2011) Hepatocellular carcinoma. *N Engl J Med* 365:1118–1127.
23. Adams PD, et al. (2010) PHENIX: A comprehensive Python-based system for macromolecular structure solution. *Acta Crystallogr D Biol Crystallogr* 66:213–221.
24. Inoki K, Li Y, Zhu T, Wu J, Guan KL (2002) TSC2 is phosphorylated and inhibited by Akt and suppresses mTOR signalling. *Nat Cell Biol* 4:648–657.
25. Wang JR, et al. (2003) Expression of LRRC4 has the potential to decrease the growth rate and tumorigenesis of glioblastoma cell line U251. *Chin J Cancer* 22:897–902.
26. Li J, et al. (2016) CD133+ liver cancer stem cells resist interferon-gamma-induced autophagy. *BMC Cancer* 16:15.
27. Ma S, Lee TK, Zheng BJ, Chan KW, Guan XY (2008) CD133+ HCC cancer stem cells confer chemoresistance by preferential expression of the Akt/PKB survival pathway. *Oncogene* 27:1749–1758.
28. Cunningham AD, Qvit N, Mochly-Rosen D (2017) Peptides and peptidomimetics as regulators of protein-protein interactions. *Curr Opin Struct Biol* 44:59–66.
29. Fosgerau K, Hoffmann T (2015) Peptide therapeutics: Current status and future directions. *Drug Discov Today* 20:122–128.
30. Walensky LD, et al. (2006) A stapled BID BH3 helix directly binds and activates BAX. *Mol Cell* 24:199–210.
31. Bruno BJ, Miller GD, Lim CS (2013) Basics and recent advances in peptide and protein drug delivery. *Ther Deliv* 4:1443–1467.
32. Moody RR, et al. (2018) Probing the interaction between the histone methyltransferase/deacetylase subunit RBBP4/7 and the transcription factor BCL11A in epigenetic complexes. *J Biol Chem* 293:2125–2136.
33. Lejon S, et al. (2011) Insights into association of the NuRD complex with FOG-1 from the crystal structure of an RbAp48·FOG-1 complex. *J Biol Chem* 286:1196–1203.
34. Liu Z, et al. (2015) Structural basis of plant homeodomain finger 6 (PHF6) recognition by the retinoblastoma binding protein 4 (RBBP4) component of the nucleosome remodeling and deacetylase (NuRD) complex. *J Biol Chem* 290:6630–6638.